

Let's take a Walk on Superpixels Graphs: Deformable Linear Objects Segmentation and Model Estimation

Daniele De Gregorio¹[0000-0001-8203-9176], Gianluca Palli²[0000-0001-9457-4643],
and Luigi Di Stefano¹[0000-0001-6014-6421]

¹ DISI, University of Bologna, 40136 Bologna, Italy

² DEI, University of Bologna, 40136 Bologna, Italy

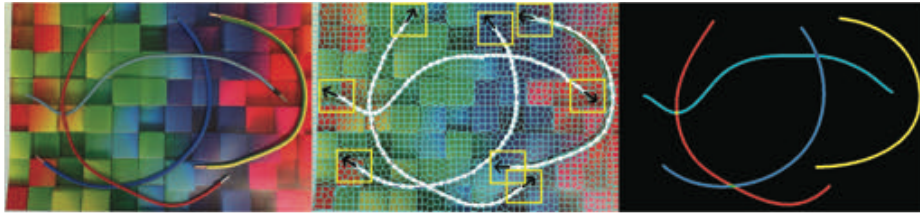


Fig. 1: Application of our algorithm to an image featuring a complex background (left). The first kind of output (center) is a *Walk* (white dots) over the Region Adjacency Graph (RAG) of the superpixel segmentation which allows for computing a b-spline model of each object. Yellow boxes highlight detection of cables terminals. The second output (right) consists in a segmentation of the whole image.

Abstract. While robotic manipulation of rigid objects is quite straightforward, coping with deformable objects is an open issue. More specifically, tasks like tying a knot, wiring a connector or even surgical suturing deal with the domain of Deformable Linear Objects (DLOs). In particular the detection of a DLO is a non-trivial problem especially under clutter and occlusions (as well as self-occlusions). The pose estimation of a DLO results into the identification of its parameters related to a designed model, e.g. a basis spline. It follows that the stand-alone segmentation of a DLO might not be sufficient to conduct a full manipulation task. This is why we propose a novel framework able to perform both a semantic segmentation and b-spline modeling of multiple deformable linear objects simultaneously without strict requirements about environment (i.e. the background). The core algorithm is based on biased random walks over the Region Adjacency Graph built on a superpixel oversegmentation of the source image. The algorithm is initialized by a Convolutional Neural Networks that detects the DLO's endcaps. An open source implementation of the proposed approach is also provided to ease the reproduction

of the whole detection pipeline along with a novel cables dataset in order to encourage further experiments.

1 Introduction

Plenty of manipulation tasks deal with objects that can be modeled as non-rigid *linear* – or more generally *tubular* – structures. In case the task has to be executed by a robot in an unstructured environment, particular effort must be devoted to effectiveness, reliability and efficiency of the automated perception sub-system. Tying knots, for example, is a common though hard to automate activity. In particular, in surgical operations like suturing, *grasp and knot-tying* is a very important and repetitive sub-task ([1][2][3]). Similar knot-tying and path planning procedures, like e.g. knots untangling, are also relevant to contexts like service, collaborative and rescue robotics ([4][5][6][7]). As for industrial scenarios, one of the hardest tasks involving flexible linear objects is wire routing in assembly processes ([8][9][10][11]). This paper focuses primarily on the industrial field and extends the original concepts introduced in the WIRES³ project and described in [12]. As the project aims at automatizing the switchgear wiring procedure, cable modeling by perception is key to address sub-tasks like cable grasp, terminal insertion, wireways routing and, not least in importance, simulation and validation.

In this paper we propose a novel computer vision algorithm for generic Deformable Linear Object (DLO) detection. As highlighted in Fig. 1, the proposed algorithm yields a twofold representation of detected objects, namely a b-spline model for each target alongside with segmentation of the whole image. This twofold representation helps addressing both relatively simpler application settings dealing with cable detection as well as more complex endeavours calling for estimation of cable bend. The proposed algorithm consists of two distinct modules: the first, which may be considered as a pre-processing stage, detects the end-caps regions of DLOs by exploiting off-the-shelf Convolutional Neural Networks ([13,14]); the second module, instead, is the core of this work and allows for identifying DLOs based on the *coarse* position of their endpoints in images featuring complex backgrounds as well as occlusions (e.g. cables crossing other cables) and self-occlusions (e.g. a cable crossing itself, also several times).

The algorithm exploits an over-segmentation of the source image into superpixels to build a Region Adjacency Graph (*RAG* [15]). This representation enables to detect the area enclosing each target object by efficiently analyzing meaningful regions (i.e. superpixels) only rather than the whole pixels set. The task is accomplished by an iterative procedure capable to find the best path (or *walk*) through the RAG between two seed points by analyzing several local and global features (e.g. visual similarity, overall curvature etc.). This iterative procedure yields a directed graph of superpixels conducive to vectorization and b-spline approximation. As better explained in the remainder of the paper,

³ This work was supported by the European Commissions Seventh Framework Programme (FP7/2007-2013) under grant agreement no. 601116.

our approach is mostly unsupervised (i.e. only the endpoints detection CNN is trained supervisedly) and relies on just a few parameters that can be easily tuned manually (or estimated based on the characteristics of object’s material, e.g. elasticity or the plasticity). As we shall see in Sec. 2, our algorithm outperforms other known approaches that one may apply to try solving the addressed task.

2 Related Work

Table 1: Curvilinear objects alongside with their key features. *Curvature* expresses the high-level shape representation for that object. *Intersections* indicates whether a crossing between two objects is allowed or not (*A* = *Allowed*, *N* = *Not*); *Bifurcations* denotes whether an object may bifurcate into multiple parts (*A*) or not (*N*).

Object Type	Curvature	Intersections	Bifurcations
Cables	Spline Model	A	N
Fingerprints	Low and Bounded	N	A
Guidewires	Spline Model	N	N
Pavement Cracks	Random	A	A
Power Lines	Spline Model	A	N
Roads	Model Based	A	A
Ropes	Spline Model	A	N
Surgery Threads	Spline Model	A	N
Vessels	Low and Bounded	N	A

Although the literature concerning DLOs is more focused on manipulation than on perception (see e.g. [3]), we may refer to the broader topic of *Curvilinear Objects Segmentation* to highlight related works as well as suitable alternatives to evaluate our proposal comparatively. As described in [16], the aforementioned topic pertains several kinds of objects, as summarized in Table 1. Our target objects are *Cables*, which, however, share similar properties in terms of *Intersections* and *Bifurcations* with the other categories highlighted in bold in Table 1,

As far as *Cables* are concerned, visual perception is typically addressed in fairly simple settings. In [17] *Augmented Reality* markers are deployed to track end-points. In other works, like [8] and [18], detection relies on background removal⁴.

Moving to the domain of knot-tying with *Ropes*, the basic approach still turns out to be background removal, like in [7], or its 3D counterpart – plane removal– like in [4] and [19]. All these methods produce a raw set of points on which a region growing algorithm is run to attain a vectorization of the target object. A different approach is used in [6], with the model of the object registered to

⁴ In [18] the authors deal with a thin flexible manipulator which may be described as a cable due to the high number of degrees of freedom.

the 3D point cloud in real-time in order to avoid the segmentation step. As described in [5], deep learning can also be used to track a deformable object: deep features are associated with rope configurations so to establish a direct mapping toward energy configurations without any explicit modeling step. This approach, however, may hardly work effectively in presence of complex and/or unknown backgrounds.

In the medical field, *Surgery Threads* detection is just the same kind of problem, albeit at a smaller scale. Also the literature dealing with this domain is more focused on manipulation than on detection issues, either assuming the latter as solved [20] or addressing it by hand-labeled markers [1]. A more scalable approach is proposed in [21] and [2], where the authors borrow the popular Frangi Filter [22] from the field of *vessels segmentation* in order to enhance the curvilinear structure of suture threads and produce a binary segmentation amenable to estimate a spline model.

Despite Table 1 would suggest *Ropes*, *Guidewires*, *Powelines* and *Surgery Threads* to exhibit more commonalities with *Cables*, applications domains like *Vessels Segmentation* or *Road detection* can provide interesting insights and solutions for curvilinear object detection. Akin to most object detection problems, the most successful approaches to *Vessels Segmentation* leverage on deep learning. In [23] the authors trained a Convolutional Neural Network (CNN) with hundreds of thousands labeled images in order to obtain a very effective detector. This supervised approach, however, mandates availability of a huge training set and lots of man-hours, a combination quite unlikely amenable to real-world industrial settings. Similar considerations apply to other remarkably effective *vessels segmentation* approaches based on supervised learning like [24] and [25]. Yet, in this realm several methods exploiting 2D filtering procedures are very popular and may be applied within a *cable* detection pipeline for industrial applications. The first interesting approach was developed by Frangi *et.al* [22] (hereinafter *Frangi* algorithm⁵) and consists in a multi-scale filtering procedure capable of enhancing tubular structures. Another methods, described in [26], deploys a pre-processing stage based on *ridge* detection (hereinafter *Ridge* algorithm⁶) to detect vessels. Although the authors use the outcome of this stage to feed a pixel-wise classifier, we found that the stage itself is very useful to highlight generic tubular structures and hence choose to compare this algorithm with ours in the experiments. Given that both the *Frangi* and *Ridge* algorithms deal with detection/enhancement of 2D curvilinear structure, we decided to include in the evaluation also *ELSD* [27], which is a popular parameter-less algorithm aimed at detection of line segments and elliptical arcs.

3 Algorithm Description

The basic idea underlying our algorithm is to detect DLOs as suitable *walks* within an adjacency graph built on superpixels. We provide first an overview of

⁵ <https://github.com/ntnu-bioopt/libfrangi>

⁶ https://github.com/kapcom01/Curvilinear_Detector

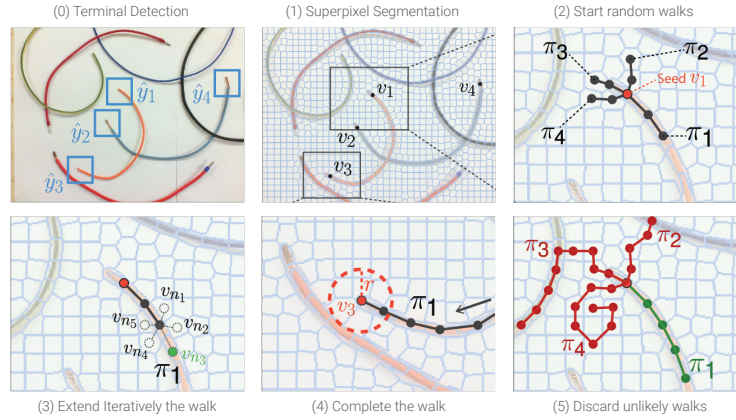
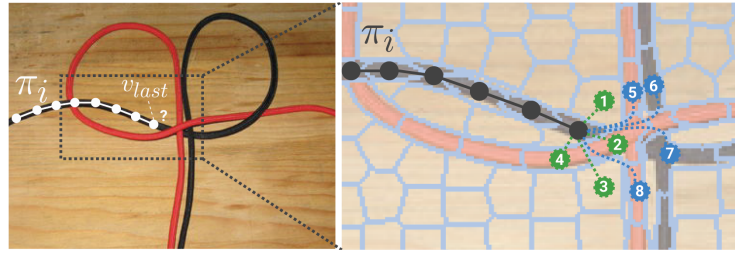


Fig. 2: A graphical representation of the whole pipeline described in detail in Sec. 3

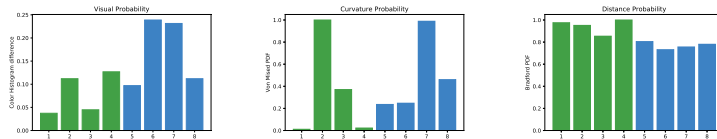
the approach with the help of Fig. 2, which illustrates the following main steps of the whole pipeline.

0. **Endpoints Detection:** The first step consists in detecting endpoints. This is numbered as zero because it may be thought of as an external process not tightly linked to the rest of the algorithm. Indeed, any external algorithm capable to produce detections around targets $(y_1 \dots y_k)$ may be deployed in this step.
1. **Superpixel Segmentation:** The source image \mathcal{I} is segmented into adjacent sub-regions (superpixels) in order to build a set of segments exhibiting a far smaller cardinality than the whole pixel set. Moreover, an adjacency graph is created on top of this segmentation in order to keep track of the neighborhood of each superpixel. Eventually, those superpixels containing the 2D detections obtained in the previous step are marked as *seeds* $(v_1 \dots v_k)$.
2. **Start Walks:** From each *seed* we can start an arbitrary number of *walks* $(\pi_1 \dots \pi_P)$ by moving into adjacent superpixels as defined by the adjacency graph.
3. **Extend Walks:** For each *walk* we move forward along the adjacency graph by choosing iteratively the best next superpixel (e.g. v_{n_3} in Fig. 2-(3)) between the neighbourhood $\{v_{n_1}, \dots, v_{n_c}\}$ of the current one.
4. **Terminate Walks:** When a *walk* reaches another *seed* (or lies in its neighborhood) it is marked as closed. Due to the iterative nature of the computation, a maximum number of extending steps is allowed for each search to ensure a bounded time complexity.
5. **Discard Unlikely Walks:** As a set of random walks are started in *Step 2*, we keep only the most likely ones and mark others as outliers.

In the remainder of this Section we will describe in detail the different concepts, methods and computations needed to realize the whole pipeline. In particular, in Sec. 3.1 we address Superpixels together with the Region Adjacency



(1) Example of crossing and self-crossing wires



(2) Visual likelihood (3) Curvature likelihood (4) Distance likelihood

Fig. 3: (1) shows a complex configuration dealing with crossing and self-crossing wires. The zoom highlights the last node (v_{last}) alongside with the candidates to select the next node, *i.e.* first and second order neighbours (green and blue dots, respectively). (2),(3) and (4) plot the Visual, Curvature and Distance likelihoods, respectively. Based on the contribution of all the three likelihood terms, node 7 is selected to extend the current *walk*.

Graph; in Sec. 3.2 we define *walks* and how they can be built iteratively by analyzing local and global features; in Sec. 3.3 we propose a method to start the random walks by exploiting an external Object Detector based on a CNN and, to conclude, in Sec. 3.4 we describe how to deploy walks to attain a semantic segmentation of the image as depicted in Fig. 1.

3.1 Superpixel Segmentation and Adjacency Graph

The main aim of *Superpixel Segmentation* is to replace the rigid structure of the pixel grid with an higher-level subdivision into more meaningful primitives called *superpixels*. These primitives group regions of perceptually similar raw pixels, thereby potentially reducing the computational complexity of further processing steps. As regards the Cable Detection and Segmentation problem (*i.e.* DLOs with a thickness higher than a single pixel, in the majority of applications), our assumptions are that the target wire can be represented as a subset of *similar* adjacent superpixels. Thus, the overall problem can be seen as a simple iterative search through the superpixels set subject to model-driven constraints (*e.g.* avoiding solutions with implausible curvature or non-uniform visual appearance).

Superpixel Segmentation algorithms can be categorized into graph-based approaches (*e.g.* the method proposed by Felzenszwalb *et al.* [28]) and gradient-ascent methods (*e.g.* *Quick Shift* [29]). In our experiments we found the state-of-

the-art algorithm referred to as *SLIC* [30] to perform particularly well in terms of both speed and accuracy. Accordingly, we deploy *SLIC* in our *Superpixel Segmentation* stage. *SLIC* is an adaptation of the *k*-means clustering algorithm to pixels represented as 5D vectors $(l_i, a_i, b_i, x_i, y_i)$, with (l_i, a_i, b_i) denoting color channels in the CIELAB space and (x_i, y_i) image coordinates. During the clustering process the compactness of each cluster can be either increased or reduced to the detriment of visual similarity. In other words we can choose easily to assign more importance to visual consistency of superpixels or to their spatial uniformity. Fig. 4 (b),(c) show two segmentations provided by *SLIC* according to different settings for the visual consistency vs. spatial uniformity trade-off.

Superpixel Segmentation allows then to build a Region Adjacency Graph (RAG in short) according to the method described in [15]. Thus, a generic image I can be partitioned into disjoint non-empty regions R_0, \dots, R_i (i.e. the superpixels) such as $I = \bigcup R_i$. Accordingly, an undirected weighted graph is given by $G = (V, E)$, where V is the set of nodes v_i , corresponding to each region R_i , and E is the set of edges $e_{j,k}$ such as that $e_{j,k} \in E$ if R_i and R_j are adjacent. A graphical representation of this kind of graph is shown in Fig. 4-(d), where black dots represents nodes v_i and black lines represent edges $e_{j,k}$. In this quite straightforward to observe that in Fig. 4-(d) there exists a *walk* through the graph G , highlighted by white dots, which covers a target DLO (i.e. the red cable in the middle).

It is worth pointing out that our approach is similar to a Region Growing algorithm, with a seed point corresponding to the cable's tip and the search space bounded by the RAG. The main difference with a classical Region Growing approach is that we restrict the search along a *walk* applying several model-base constraints rather than relying only on visual similarity only. In particular, the shape of the *walk* is considered by assigning geometric primitives to the elements of the adjacency graph, i.e. 2D points for our nodes v_i and 2D segments for our edges $e_{j,k}$, as further described in Sec. 3.2. In simple terms, the geometric consistency of the curve superimposed on a *walk* is analyzed to choose the next node during the iterative search, and all unlikely configurations are discarded.

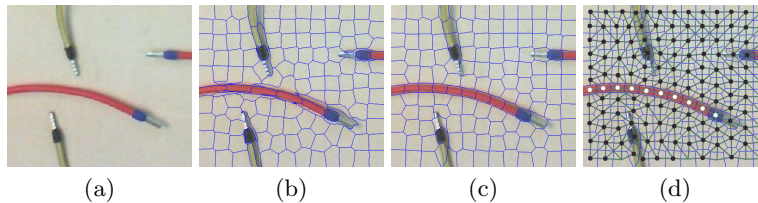


Fig. 4: (a) Original input image. (b) SLIC superpixels segmentation with low compactness. (c) Segmentation with high compactness. (d) The Region Adjacency Graph (RAG) built on the (c) segmentation.

3.2 Walking on the Adjacency Graph

Formally, a walk over a graph $G = (V, E)$ is a sequence of alternating vertices and edges $(v_{i_1}, e_{i_1, i_2}, v_{i_2}, \dots, v_{i_{l-1}}, e_{i_{l-1}, i_l}, v_{i_l})$, where an edge e_{i_j, i_k} connects nodes v_{i_j} and v_{i_k} , and l is the length of the walk. The definition of *walk* is more general with respect to the *path* or *trail* over the graph because it admits repeated vertices, a common situation when dealing with self-crossing cables. It is important to notice that the Region Adjacency Graph shown in Fig. 4(d) is a *simple-connectivity relationship* graph, or, equivalently, connectivity is of order $d = 1$, with this meaning that only directly connected regions are mapped into the graph. We can build also RAGs with order $d > 1$, thereby allowing, for example, second or third order connectivity. All this translates into the possibility to *jump* during the walk also to the vertex not directly connected to the current region. This turns out very useful, for example, to deal with intersections like that depicted in Fig. 3, where vertices v_1, v_2, v_3, v_4 are of order $d = 1$ and vertices v_5, v_6, v_7, v_8 of order $d = 2$.

For the sake of simplicity, we can define a generic *walk* as $\pi_i = (v_{i_1}, \dots, v_{i_l})$, i.e. an ordered subset of vertices, without considering edges. Under the hypothesis that the target walk π_i is superimposed to a portion of the object, the problem is to *extend* the walk in such a way that the next node $v_{i_{l+1}}$ does belong to the sought DLO. An exemplar situation is illustrated in Fig. 3, where we have a current path π_i which ends with v_{last} and we wish to choose between the 8 vertices the best one to extend the *walk*. Considering the new path $\hat{\pi}_{i, v_n}$, i.e. the path π_i with the addition of vertex v_n , we cast the problem as the estimation of the likelihood of the new path given the current one, which we denote as $p(\hat{\pi}_{i, v_n} | \pi_i)$. Moreover, we estimate this likelihood based on visual similarity, curvature smoothness and spatial distance features and assume these features to be independent:

$$p(\hat{\pi}_{i, v_n} | \pi_i) = p_V(\hat{\pi}_{i, v_n} | \pi_i) \cdot p_C(\hat{\pi}_{i, v_n} | \pi_i) \cdot p_D(\hat{\pi}_{i, v_n} | \pi_i) \quad (1)$$

The three terms $p_V(\cdot)$, $p_C(\cdot)$ and $p_D(\cdot)$ are referred to as *Visual*, *Curvature* and *Distance* likelihood, respectively, and computed as follows.

Visual Likelihood $p_V(\hat{\pi}_{i, v_n} | \pi_i)$ measures the visual similarity between the previous path π_i and the path achievable by adding node v_n . Assuming an evenly coloured DLO, we can compute this similarity by matching only the last node of π_i , v_{last} , with v_n . Although, in principle, it may be possible to use any arbitrary visual matching function, as highlighted in [31] we found the Color Histogram of the superpixels associated with vertices to be a good feature to compare two image regions. Denoting as H_{last} and H_n the normalized color histograms (in the HSV color space) of the two regions associated with v_{last} and v_n , respectively, we can compute their distance with the intersection equation:

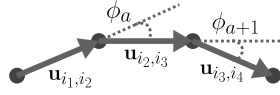


Fig. 5: A generic unit vector \mathbf{u} can be assigned to each edge in the adjacency graph so as to compute the angle difference ϕ_a , between consecutive edges.

$d(H_{last}, H_n) = \sum_I \min(H_{last}(I), H_n(I))$. Then we normalize this distance in the range $[0, 1]$ using the *Bradford* normal distribution:

$$p_V(\hat{\pi}_{i,v_n} | \pi_i) = \frac{c_V}{\log(1 + c_V)(1 + c_V(1 - d(H_{last}, H_n)))} \quad (2)$$

where c_V is a parameter that enables to control the shape of the distribution and, hence, the weight assigned to the visual similarity information in the overall computation of the likelihood (Eq. 1). Fig. 3(2) plots the visual likelihoods computed for the different neighbours of v_{last} , which suggests nodes 6 and 7 to represent the most likely superpixels to extend the *walk*.

Curvature Likelihood $p_C(\hat{\pi}_{i,v_n} | \pi_i)$ is concerned with estimating the most likely configuration of a DLO's curvature. Following the intuitions of Predoehl *et al.* [32], for each new node v_n we can assume that the object's curvature changes smoothly along the *walk*. To quantify this smoothness criterion we exploit the product of the von Mises distributions of the angles between two successive vertices. As introduced in Sec. 3.1, by extending the model of our adjacency graph with geometric primitives we can assign a 2D point \mathbf{p}_{i_j} corresponding to the centroid of the associated superpixel to each vertex v_{i_j} , as well as a unit vector $\mathbf{u}_{i_j,k}$ to each edge $e_{i_j,k}$ by considering the segment joining two consecutive centroids \mathbf{p}_{i_j} , \mathbf{p}_{i_k} . As shown in Fig. 5, this allows for measuring the angle difference between two consecutive edges. By denoting as $\phi_a = \phi_{j,k,m}$ the angle difference between two consecutive edges $\mathbf{u}_{i_j,k}$, $\mathbf{u}_{i_k,m}$, the overall von Mises distribution allowing to establish upon the smoothness of the curvature of a target DLO is given by:

$$p_C(\hat{\pi}_{i,v_n} | \pi_i) = \prod_a \mathcal{M}\left(\frac{\phi_a - \phi_{a+1}}{2}, m\right) \quad (3)$$

where $\mathcal{M}(\cdot)$ is the von Mises distribution at each vertex. An exemplar estimation is shown in Fig. 3(3): vertices 2 and 7 appear to be the most likely candidates to extend the *walk* as they minimize the curvature changes of the target π_i .

Distance Likelihood $p_D(\hat{\pi}_{i,v_n} | \pi_i)$ is the term concerned with the spatial distance of the next vertex in the *walk*. This term is mainly introduced to force the iterative procedure to choose the nearest available vertex without undermining the chance to pick a far vertex instead, for example when we want to deal with

an intersection (see Fig. 3(1)). Thus, similarly to Eq. 3.2 we normalize the distance in pixel between two nodes, $d_{pixel}(\mathbf{p}_{i_{last}}, \mathbf{p}_{i_n})$, according to the Bradford normal distribution:

$$p_D(\hat{\pi}_{i,v_n}|\pi_i) = \frac{c_D}{\log(1 + c_D)(1 + c_D(1 - d_{pixel}(\mathbf{p}_{i_{last}}, \mathbf{p}_{i_n}))} \quad (4)$$

with c_D tuned such that the decay of the distribution is slow to prefer nearest vertex but not enough to discard the furthest points. Fig. 3(4) highlights how, thanks to the normalization in Eq. 3.2, second order neighbours (5, ..., 8) are not excessively penalized with respect to first order ones (1, ..., 4) and hence have the chance to be picked in case they exhibit a high visual similarity and/or yield a particularly smooth *walk*.

Estimation of the most likely walk $p(\hat{\pi}_{i,v_n}|\pi_i)$ can therefore be computed for all considered neighbours in order to pick the most likely vertex, v_n , to extend the *walk*, with:

$$n = \arg \max_n p(\hat{\pi}_{i,v_n}|\pi_i) \quad (5)$$

Considering again the example in Fig. 3, although the farthest from v_{last} , vertex 7 is selected to extend the *walk* as it shows a high visual likelihood as well as a high curvature likelihood.

3.3 Starting and Terminating Walks

As described Sec. 3, *walks* need to be initialized with *seed* superpixels located at DLOs' endpoints. Purposely, we deployed a Convolutional Neural Network to detect endpoints. In particular, we fine-tuned the publicly available YOLO v2 model [13] pre-trained on ImageNet based on the images from our *Electrical Cable Dataset* (see Sec. 4.1) and by performing several data augmentations. As already mentioned, the endpoint detection module may be seen as an external process with respect to our core algorithm and, as such, in the comparative experimental evaluation we will use the same set of endpoints obtained by YOLO v2 to initialize all considered methods.

As illustrated in Fig. 2(1), the endpoint detection step predicts a set of bounding boxes \hat{y}_i around the actual endpoints. For each such prediction we find the superpixel containing the central point of the box. The graph vertex v_i corresponding to this superpixel is marked as a *seed* to start a new *walk*. As no prior information concerning the direction of the best *walk* across the target DLO is available, multiple *walks* are actually started, in particular along each possible direction (see Fig. 2(3)). It is worth pointing out that the considered directions are those defined by the *seed* vertex and all its neighbours in the graph, which, as discussed in Sec. 3.2, can be both first order ($d = 1$) as well as higher order

($d > 1$) neighbours. Each started *walk*, then, is iteratively extended according to the procedure described in Sec. 3.2. .

As for the criteria to terminate *walks*, first of all we set a maximum number of iterations to extend a *walk*. We also terminate a *walk* if it reaches another *seed* vertex in the adjacency graph. More precisely, as depicted in Fig. 2(5), we terminate a *walk* if the distance from the current vertex and a *seed* is smaller than a radius threshold r . Thus, given a *seed*, all *walks* started from that *seed* will terminate and we will have to pick only the optimal one. Purposely, we exploit again the *Curvature* analysis described in Sec. 3.2 and use a formulation similar to Eq. 3 to pick the smoothest path (i.e. the *walk* with the highest value of $P_C(\cdot)$).

3.4 Segmentation and Model Estimation

The simplest technique to segment the image is to assign different labels to the superpixels belonging to the different *walks* alongside with a background label to those superpixels not included into any *walk*. Besides, we estimate a B-Spline approximation (with the algorithm described in [33]) for each walk based on the centroids of the its superpixels $\mathbf{p}_0, \dots, \mathbf{p}_l$. Then, given the B-Spline model we can refine the segmentation by building a pixel mask. In particular, by evaluating the smoothing polynomial we can sample densely the points belonging to each parametrised curve and then adjust the thickness of the segmented output based on the mean size of the superpixels belonging to the *walk*. The accurate segmentation provided by this procedure is shown in Fig. 1, where the right image contains the colored B-Splines built over the walks represented in the middle image (the color is estimated by averaging the color of the corresponding superpixels).

4 Experimental results

4.1 Software and Dataset

We provide an open source software framework called *Ariadne* available online ⁷. The name *Ariadne* is inspired by the name of Minos’s daughter, who, in Greek mythology, used a thread to lead Theseus outside the Minotaur’s maze. The software is written in Python and implements the described approach. We created also a novel dataset ⁸ which, to the best of our knowledge, is the first *Electrical Cable* dataset for detection and segmentation. We used this dataset to perform quantitative and qualitative evaluations of our approach with respect to others curvilinear structure detector.

The Dataset is made up of two separated parts: the first consists of 60 cable images with homogeneous backgrounds (white, wood, colored papers, etc.); the

⁷ <https://github.com/m4nh/ariadne>

⁸ https://github.com/m4nh/cables_dataset

second includes 10 cable images with complex backgrounds. In Fig. 7, the first 3 rows deal with homogenous backgrounds whilst the other with complex one.

For each image in the dataset we provide an hand-labeled binary mask superimposed over each target cable separately and an overall mask that is the union of them. Furthermore, we provide a discretization of the B-Spline for each cable in every image which consists in a set of 2D points in pixel coordinates useful to have a lighter model of the cable and track easily its endings. Further details can be found on the dataset website ⁹.

4.2 Segmentation results

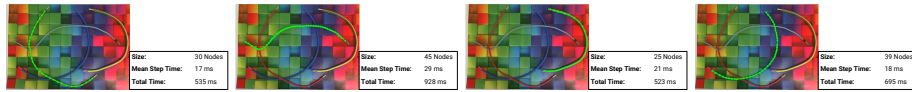


Fig. 6: Segmentation timings (complex background).

To test our approach we compared it to the popular Curvilinear Object Detector discussed in Sec. 2: the Frangi 2D Filter [22], the Ridge Algorithm [26] and the more generic one ELSD [27]. For each algorithm we produce a mask $M_{prediction}$ associated with the detected curvilinear structures and compare it, by means of the Intersection Over Union, $IoU = \frac{M_{gt} \cap M_{prediction}}{M_{gt} \cup M_{prediction}}$, to the ground truth M_{gt} provided by our dataset. Table 1 reports the weighted IoU on N images, where the weight is proportional to the number of cables C present in the image: $IoU_{weighted} = \frac{1}{C \cdot N} \sum_i C \cdot IoU_i$. The first row refers to images featuring a homogeneous background (60 images with a total of 395 cables), the second to those having a complex background (10 images and a total of 40 cables). We tuned the hyperparameters of the three competing methods trying to choose the best configuration in order to cope with both the simpler and harder dataset images. As for our algorithm, we used: a 3D Color Histogram with 8 bins for each channel as Visual similarity feature; a Von Mises distribution with $m = 4$ to compute the Curvature likelihood and a degree $d = 3$ for the adjacency graph (i.e. it means that we search in a neighborhood of level 3 during our walk construction, as described in Sec. 3.2). For both our approach and the competitors we exploit the information about the endpoints provided by the initialization step: for *Ariadne* we use this information to start random walks, for the competitors to discard many outliers.

The results reported in Table 1 show how our approach outperforms the other methods by a large margin, although it is fair to point out that the competitors are generic curvilinear detectors and not specific DLO detectors. It is also worth highlighting that our method is remarkably robust with respect to complex backgrounds and that this is achieved without any training or fitting procedure that would hinder applicability to unknown scenarios. Thus, our approach could be

⁹ https://github.com/m4nh/cables_dataset

used in any real industrial application without requiring prior knowledge of the environment.

Finally, Fig. 7, present some qualitative results obtained by our approach. Moreover, an additional qualitative evaluation is present in the supplementary material, where interactive examples of the Ariadne software are shown. In the abovementioned material, as a naive proof-of-concept, we tested Ariadne also in similar challenging contexts like *Roads* and *Rivers* segmentation.

Table 2: The Intersection Over Union of the cable segmentations obtained with our approach compared with the three major curvilinear structure detectors.

	Ariadne	Frangi [22]	Ridge [26]	ELSD [27]
Homegeneous Background	0.754	0.406	0.293	0.225
Complex Background	0.583	0.063	0.023	0.147

4.3 Timings and failure cases

Ariadne is an iterative approach, with the number of iterations depending on the length of the DLO. Thus, as depicted in Fig. 6, we can estimate an average iteration time of about $21ms$ and an average segmentation time of about $670ms$. We also point out that these measurements were obtained with the actual Python implementation. Moreover, Fig. 8(a),(b) shows the two main failure cases that we found for *Ariadne*. In (a), as two DLOs (blue and green) are adjacent and exhibit very similar colour and curvature, the walk may jump on the wrong cable. In (b), as the distance between the DLO and the camera varies greatly, the density of Superpixels is not constant and the walk can cover only a portion of the sought object or even completely fail.

5 Concluding Remarks

We presented an effective unsupervised approach to segment DLOs in images. This segmentation method may be deployed in industrial applications involving wire detection and manipulation. Our approach requires an external detector to localize cable terminals, as otherwise we should start *walks* at every superpixel, which would be almost unworkable, although not impossible. So far we deploy an external detector which provides only the approximate position of the endpoints. We are currently working to develop a smarter endpoint detector capable to infer also the orientation of the cable terminal in order to dramatically shrink the number of initial *walks*. Another future development concerns building a much larger Electrical Cable dataset equipped with ground truth information suitable to train a specific CNN aimed at cable segmentation and compare this supervised

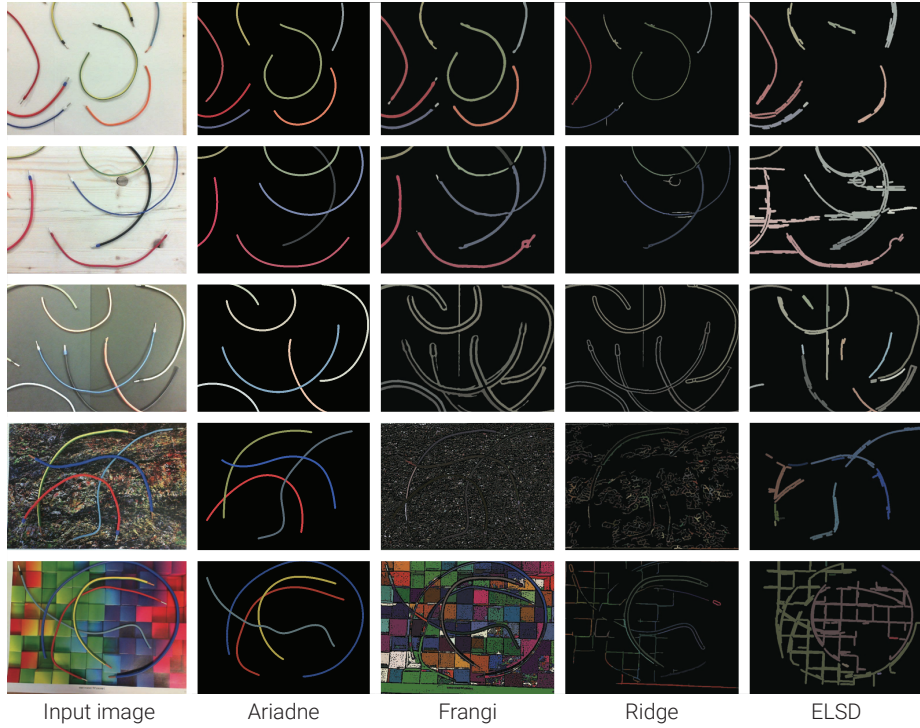
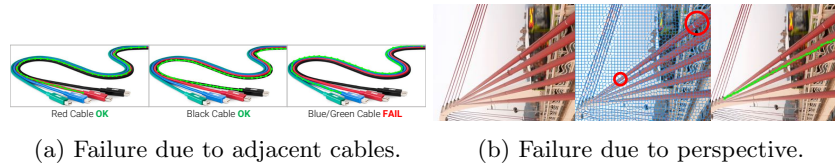


Fig. 7: Qualitative evaluation of the different algorithms. The first column represent the input image, whereas the other columns, in order: the result yielded by *Ariadne*, *Frangi*[22], *Ridge*[26] and *ELSD*[27]. The difficulty increases from a row to the following: indeed the first row represent a very simple example with white background while the last example, instead, can be considered very hard. Our approach is very robust despite background complexity.

approach to *Ariadne*. It is worth pointing out that, in specific and known in advance settings, a supervised approach may turn out peculiarly effective: in such circumstances *Ariadne* could be used to vastly ease and speed up the manual labeling procedure required to obtain the training images by replacing the initial object detector with the interactive intervention of the user.



(a) Failure due to adjacent cables.

(b) Failure due to perspective.

Fig. 8: Failure Cases.

References

1. Javdani, S., Tandon, S., Tang, J., O'Brien, J.F., Abbeel, P.: Modeling and perception of deformable one-dimensional objects. In: *Robotics and Automation (ICRA)*, 2011 IEEE International Conference on, IEEE (2011) 1607–1614
2. Jackson, R.C., Yuan, R., Chow, D.L., Newman, W., Çavuşoğlu, M.C.: Automatic initialization and dynamic tracking of surgical suture threads. In: *Robotics and Automation (ICRA)*, 2015 IEEE International Conference on, IEEE (2015) 4710–4716
3. Saha, M., Isto, P.: Manipulation planning for deformable linear objects. *IEEE Transactions on Robotics* **23** (2007) 1141–1150
4. Lui, W.H., Saxena, A.: Tangled: Learning to untangle ropes with rgb-d perception. In: *Intelligent Robots and Systems (IROS)*, 2013 IEEE/RSJ International Conference on, IEEE (2013) 837–844
5. Nair, A., Chen, D., Agrawal, P., Isola, P., Abbeel, P., Malik, J., Levine, S.: Combining self-supervised learning and imitation for vision-based rope manipulation. *Robotics and Automation (ICRA)*, 2017 IEEE International Conference on (2017) 2146–2153
6. Schulman, J., Lee, A., Ho, J., Abbeel, P.: Tracking deformable objects with point clouds. In: *Robotics and Automation (ICRA)*, 2013 IEEE International Conference on, IEEE (2013) 1130–1137
7. Hopcroft, J.E., Kearney, J.K., Krafft, D.B.: A case study of flexible object manipulation. *The International Journal of Robotics Research* **10** (1991) 41–50
8. Remde, A., Henrich, D., Wörn, H.: Picking-up deformable linear objects with industrial robots. (1999)
9. Yue, S., Henrich, D.: Manipulating deformable linear objects: sensor-based fast manipulation during vibration. In: *Robotics and Automation, 2002. Proceedings. ICRA'02. IEEE International Conference on. Volume 3.*, IEEE (2002) 2467–2472
10. Alvarez, N., Yamazaki, K., Matsubara, T.: An approach to realistic physical simulation of digitally captured deformable linear objects. In: *Simulation, Modeling, and Programming for Autonomous Robots (SIMPAN)*, IEEE International Conference on, IEEE (2016) 135–140
11. Koo, K.m., Jiang, X., Kikuchi, K., Konno, A., Uchiyama, M.: Development of a robot car wiring system. In: *Advanced Intelligent Mechatronics, 2008. AIM 2008. IEEE/ASME International Conference on*, IEEE (2008) 862–867
12. Gregorio, D.D., Zanella, R., Palli, G., Pirozzi, S., Melchiorri, C.: Integration of robotic vision and tactile sensing for wire-terminal insertion tasks. *IEEE Transactions on Automation Science and Engineering* (2018) 1–14
13. Redmon, J., Farhadi, A.: Yolo9000: Better, faster, stronger. In: *Computer Vision and Pattern Recognition (CVPR)*, 2017 IEEE Conference on, IEEE (2017) 6517–6525
14. Huang, J., Rathod, V., Sun, C., Zhu, M., Korattikara, A., Fathi, A., Fischer, I., Wojna, Z., Song, Y., Guadarrama, S., et al.: Speed/accuracy trade-offs for modern convolutional object detectors. (2017)
15. Trémeau, A., Colantoni, P.: Regions adjacency graph applied to color image segmentation. *IEEE Transactions on image processing* **9** (2000) 735–744
16. Bibiloni, P., González-Hidalgo, M., Massanet, S.: A survey on curvilinear object segmentation in multiple applications. *Pattern Recognition* **60** (2016) 949–970
17. Jiang, X., Koo, K.m., Kikuchi, K., Konno, A., Uchiyama, M.: Robotized assembly of a wire harness in a car production line. *Advanced Robotics* **25** (2011) 473–489

18. Camarillo, D.B., Loewke, K.E., Carlson, C.R., Salisbury, J.K.: Vision based 3-d shape sensing of flexible manipulators. In: *Robotics and Automation, 2008. ICRA 2008. IEEE International Conference on*, IEEE (2008) 2940–2947
19. Schulman, J., Ho, J., Lee, C., Abbeel, P.: Learning from demonstrations through the use of non-rigid registration. In: *Robotics Research*. Springer (2016) 339–354
20. Moll, M., Kavraki, L.E.: Path planning for deformable linear objects. *IEEE Transactions on Robotics* **22** (2006) 625–636
21. Padoy, N., Hager, G.D.: 3d thread tracking for robotic assistance in tele-surgery. In: *Intelligent Robots and Systems (IROS), 2011 IEEE/RSJ International Conference on*, IEEE (2011) 2102–2107
22. Frangi, A.F., Niessen, W.J., Vincken, K.L., Viergever, M.A.: Multiscale vessel enhancement filtering. In: *International Conference on Medical Image Computing and Computer-Assisted Intervention*, Springer (1998) 130–137
23. Liskowski, P., Krawiec, K.: Segmenting retinal blood vessels with deep neural networks. *IEEE transactions on medical imaging* **35** (2016) 2369–2380
24. Melinščak, M., Prentašić, P., Lončarić, S.: Retinal vessel segmentation using deep neural networks. In: *VISAPP 2015 (10th International Conference on Computer Vision Theory and Applications)*. (2015)
25. Li, Q., Feng, B., Xie, L., Liang, P., Zhang, H., Wang, T.: A cross-modality learning approach for vessel segmentation in retinal images. *IEEE transactions on medical imaging* **35** (2016) 109–118
26. Staal, J., Abràmoff, M.D., Niemeijer, M., Viergever, M.A., Van Ginneken, B.: Ridge-based vessel segmentation in color images of the retina. *IEEE transactions on medical imaging* **23** (2004) 501–509
27. Pătrăucean, V., Gurdjos, P., Von Gioi, R.G.: A parameterless line segment and elliptical arc detector with enhanced ellipse fitting. In: *Computer Vision–ECCV 2012*. Springer (2012) 572–585
28. Felzenszwalb, P.F., Huttenlocher, D.P.: Efficient graph-based image segmentation. *International journal of computer vision* **59** (2004) 167–181
29. Vedaldi, A., Soatto, S.: Quick shift and kernel methods for mode seeking. In: *European Conference on Computer Vision*, Springer (2008) 705–718
30. Achanta, R., Shaji, A., Smith, K., Lucchi, A., Fua, P., Süsstrunk, S.: Slic superpixels compared to state-of-the-art superpixel methods. *IEEE transactions on pattern analysis and machine intelligence* **34** (2012) 2274–2282
31. Ning, J., Zhang, L., Zhang, D., Wu, C.: Interactive image segmentation by maximal similarity based region merging. *Pattern Recognition* **43** (2010) 445–456
32. Predoehl, A., Morris, S., Barnard, K.: A statistical model for recreational trails in aerial images. In: *Computer Vision and Pattern Recognition (CVPR), 2013 IEEE Conference on*, IEEE (2013) 337–344
33. Dierckx, P.: *Curve and surface fitting with splines*. Oxford University Press (1995)